Realistic ray-tracing model of a Scheffler reflector based on experimental data

Thomas Fasquelle, Benjamin Kadoch, Gabriel Guillet, Séverine Barbosa

Renewable Energy 231 (2024) 120856

Contents lists available at ScienceDirect

Renewable Energy

journal homepage: www.elsevier.com/locate/renene

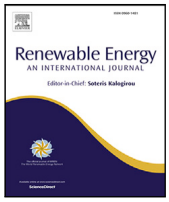

Realistic ray-tracing model of a Scheffler reflector based on experimental data

Thomas Fasquelle *, Benjamin Kadoch, Gabriel Guillet, Séverine Barbosa

Aix Marseille Univ, CNRS, IUSTI, Marseille, France

ARTICLE INFO

Keywords:
Concentrated solar power
Scheffler reflectors
Monte-Carlo ray-tracing
Sensitivity analysis

ABSTRACT

A model of a Scheffler reflector with mirror facets is presented in the form of an open-source script for use with the free ray-tracing software Soltrace (Monte-Carlo method). It is calibrated to match the experimental results obtained with an 8 m^2 (surface area) reflector of 1.43 m focal distance. It is found that the optical errors of real reflectors (slope, specularity, shape) are very large, leading to results that are far from theoretical. A sensitivity study is then carried out to assess the level of importance of reflector and receiver positioning and adjustment to obtain maximum performance. The parametric study showed that the margin of error is quite small for north–south alignment, rotation axis adjustment, horizontal receiver position, declination adjustment and tracking system, with a performance reduction of 10% for errors of 1°, 0.8°, 6 cm, 2 days and 4 min, respectively. The inclination of the receiver has lower influence on the results. The performance of Scheffler reflectors could therefore be greatly enhanced by improving the shape and characteristics of the mirrors, taking particular care with the various settings. In addition, as an application example, a secondary optical system multiplying the power density by up to 3.3 is proposed.

1. Introduction

The decarbonization of human society requires the use of renewable energies such as wind and solar. In the latter case, a wide range of technologies coexist and can be separated into three families: photovoltaics, non-concentrated solar thermal systems and concentrated solar systems. The latter have the advantage of being able to reach high temperatures, *e.g.* 3500 °C [1], with a relatively high solar-to-heat efficiency (40%-70%), where photovoltaic systems directly produce electricity but at a low efficiency (~20% for commercial single-junction silicon cells) and non-concentrated solar systems are limited to low temperatures (typically <200 °C). The disadvantages of concentrating systems are (i) cost; (ii) the need for direct solar radiation; (iii) the need for a complex and accurate tracking system that moves both the reflector and receiver [2].

Scheffler reflectors, whose concept is illustrated in Figs. 1 and 2, are a special type of concentrators that have the great advantage of a fixed focus while the reflector moves around it during the day or changes shape throughout the year. This concept was created by Wolfgang Scheffler in a "low-tech" spirit, allowing the population to build and maintain the system with relatively common materials and skills [3,4]. Scheffler reflectors are positioned and adjusted manually, thanks to simple tools such as levels, compass and integrated extensible arms. Scheffler reflectors combined with properly insulated receiver enable the latter to reach temperatures of up to 800 °C [5] and can be used for a variety of applications [6,7] such as baking bread, generating steam for cooking [8], distillation [9], electricity generation [10], or even air conditioning and sterilization [11].

Since Wolfgang Scheffler's first communications on this technology, his reflector has spread all over the world and especially in India [12,13]. However, scientific studies dealing with its operating principle, its performance, its modeling and its improvement have been quite rare. In fact, to the best of our knowledge, the first paper dealing with its design was published by Munir et al. in 2010 [14]. In 2018, Reddy et al. completed the previous work by giving a comprehensive methodology to build a Scheffler reflector [15], and even proposed new designs supported by a simple ray tracing MATLAB code [16]. The latter uses geometric optics and can estimate the size of the Scheffler's image but it does not give details on power distribution. Actually, efficient and versatile modeling codes are scarce, and they have rarely been validated by experimental results, as the number of complete performance characterization and details on focal images is also limited. For instance, Ruelas et al. [17,18] developed a ray-tracing code for a Scheffler-type reflector to help design their absorber, however their numerical reflector is non-deformable. Some other authors developed rather complete models but using proprietary softwares: Sasidharan et al. [19]

* Corresponding author.
E-mail address: thomas.fasquelle@univ-amu.fr (T. Fasquelle).

https://doi.org/10.1016/j.renene.2024.120856
Received 29 February 2024; Received in revised form 15 June 2024; Accepted 20 June 2024
Available online 26 June 2024

Nomenclature

Latin symbols

A_{sc}	Surface area of the reflector m^2
A_{im}	Surface area of the focal image m^2
A_{ap}	Aperture area of the reflector m^2
B_1	Major axis of the Scheffler reflector m
B_2	Minor axis of the Scheffler reflector m
CR	Concentration Ratio
d	Receiver's horizontal distance error to the focal point in the design of experiment
$d1$	Delay in the daily adjustment error in the design of experiment
$d2$	Delay in the tracking angle error in the design of experiment
DNI	SolarDirect Normal Irradiance $W\,m^{-2}$
f	Focal distance of the parabola m
f_n	Daily focal distance of the parabola m
k_{sun}	Multiplication factor applied to the angular radius of the Sun
lat	Latitude of the location °
N	Number of parameters in the design of experiment
P_{rec}	Total power received by a hypothetical flat disk receiver with a 26 cm diameter W
P_{tot}	Total power received by the arbitrary flat square 1 m^2 target/receiver W
R	Name of the error of rotation axis' angle in the design of experiment
(R_x, R_y, R_z)	Rotations around the global or local axes
S	Scheffler reflector's horizontal orientation error in the design of experiment
SS_i	Sum of square for an effect in the design of experiment
SST	Total sum of squares for all effects in the design of experiment
(x, y, z)	Global coordinate system m
(x^*, y^*, z^*)	Local coordinate systems m
x_i	Non-normalized system output for the design of experiment
X_i	Normalized system output for the design of experiment
X_{ref}	Reference output for the design of experiment
y_i	Output objective in the design of experiment

Greek symbols

α	Inclination angle of the Scheffler reflector at design °
β	Inclination angle of the receiver °
$\hat{\beta} = \beta_i$	Effect of a parameter variation in the design of experiment °
δ	Solar declination angle °
ϵ_{lat}	Error on the inclination of the reflector's rotation axis °
ϵ_{dis}	Error on the horizontal position of the receiver m
ϵ_{South}	Error on the horizontal orientation of the Scheffler reflector °
ϵ_β	Error on the receiver's inclination angle °
ϵ_δ	Error on the daily adjustment of the reflector °
ϵ_ω	Error on the tracking angle of the reflector °
θ_{Sun}	Angular apparent radius of the Sun °
$\rho_{mirrors}$	Reflectivity of mirrors
σ_{shape}	Optical error due to wrong local shape of the reflector °
σ_{slope}	Optical error due to wrong local slope of the reflector °
σ_{spec}	Optical error due to non-perfectly specular mirrors °
σ_{Sun}	Optical error due to the finite size of the Sun °
σ_{tot}	Total optical error of the system °
$\sigma_{tracking}$	Optical error due to wrong tracking angle of the reflector °
$\langle\phi\rangle$	Average power density received by the receiver $W\,m^{-2}$

used a 3D CAD software and the module "Ray Optics" from ComSol Multiphysics to estimate their experimental power distribution, however the capabilities and limitations of their tool are not clear. The same goes for Fontani et al. [20] who used SolidWorks and Zemax-OpticStudio to understand the effect of the mechanical deformations on the irradiance maps and size their receiver.

In a previous paper [21], we tried to partially fill the experimental data gap and qualitatively compared our results with the extensive work of Dib et al. [22]. Using this experimental knowledge, the present work provides an open-source code (shared on a dedicated platform) under Soltrace software [23] to allow the scientific community to perform Monte-Carlo-Ray-Tracing (MCRT) simulations of Scheffler reflectors. Soltrace has been developed by the National Renewable Energy Laboratory (NREL) and is one of the most used ray-tracing software for Concentrating Solar Power (CSP) applications, such as central receivers [24], parabolic troughs [25], Fresnel linear reflectors [26] and even some solar cookers [27]. It has the advantage of being open-source, free, versatile and allows parametric studies and post-processing with other softwares. It has some drawbacks such as the impossibility to upload CAD models, or the fact that it does not include an attenuation coefficient for central receivers [24] (although an analog version is used for this purpose in the Solar Pilot open-source software from NREL, that is dedicated to central receivers [28]). Because it uses MCRT, Soltrace is a reliable tool to predict power distribution of solar collectors in a relatively low computing time.

Another novelty of this work is the study and quantification of the influence of optical and adjustment errors on Scheffler reflector performance.

The following sections are structured as follows: (i) Methodology with the main equations and the main parameters of interest; (ii) Adjustment of the optical parameters to fit our experimental data; (iii) Parametric studies to evaluate the margin for errors in the Scheffler reflector positioning and adjustment; (iv) Design of a possible secondary optical system; (v) Conclusions and perspectives.

2. Methodology

The Soltrace script that is provided with this article generates a model of a Scheffler reflector with mirror facets and with potential adjustment errors that are depicted in Fig. 1. The following subsections deal with the different inputs and equations used, following the theoretical aspects that have been formulated by Reddy et al. [15] (see Appendix A for the slight differences between our models).

2.1. Main inputs

The three main inputs, defined as in [15] (see Fig. 2) are:

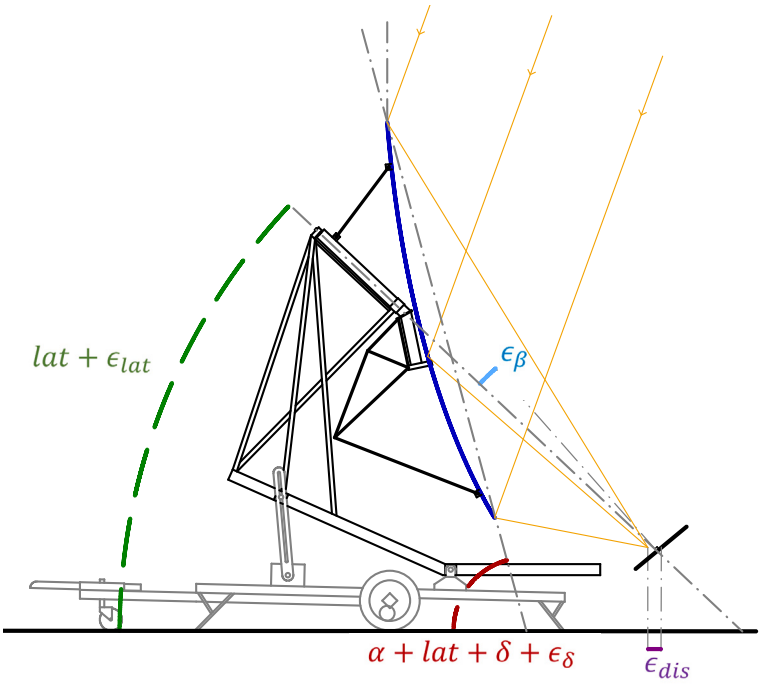

Fig. 1. Representation of a Scheffler reflector (in dark blue) with errors on four adjustment parameters: ϵ_{lat} (for inclination of the rotation axis), ϵ_δ (inclination of the reflector), ϵ_{dist} (horizontal position of the receiver) and ϵ_β (inclination of the receiver).

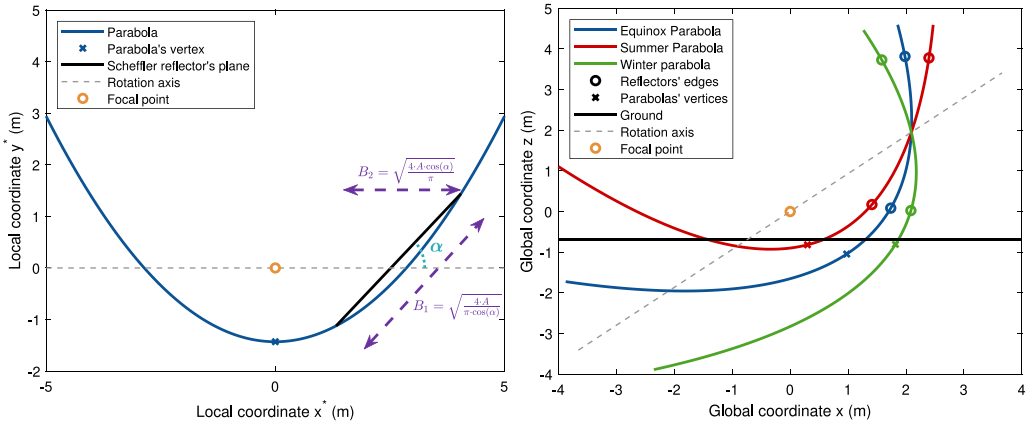

Fig. 2. Construction of a Scheffler reflector: intersection of a parabola and a plane, local coordinate system (a). Position of a Scheffler reflector located in $lat = 43°$, with an 8 m^2 aperture and a 1.43 m focal distance, for the equinoxes and the solstices, global coordinate system (b).

- the focal length of the parabola at the equinox f;
- the inclination of the Scheffler reflector aperture plane at design point α, which defines the part of the imaginary parabola that will be approximated by a curved plane, and which should lead to the lowest torque for the steel structure;
- the desired elliptical surface area $A_{sc} = \pi \cdot \frac{B_1 \cdot B_2}{4}$ and the desired aperture area $A_{ap} = \pi \cdot \frac{B_2^2}{4}$ of the reflector, with B_1 and B_2 the minor and major axes of the ellipse, respectively, and with $B_2 = B_1 \cdot \cos(\alpha)$.

In addition, one should specify the solar Direct Normal Irradiance (DNI), the reflectivity of the mirrors, the receiver characteristics, the location and time and the different optical errors.

2.2. Determination of the position of the paraboloid's facet and the receiver

The Scheffler reflector is created out of the intersection between a paraboloid and an inclined plane, in a cartesian coordinate system (O, x, y, z) and with the focal point as origin. The former is created considering the Sun is exactly on its Zenith (Equator line, Equinox, solar noon), then it is rotated several times to match the exact location and time. In this coordinate system, the general equation of a paraboloid oriented towards its zenith, with a focal distance at equinox f, is the following:

$$z^*(x, y, z) = \frac{x^2 + y^2}{4 \cdot f} - f \tag{1}$$

To get a fixed receiver, the paraboloid shape is changed with respect to the chosen day number n (from 1 to 365), parameterized by the declination angle δ. Its focal distance is therefore variable and defined by Eq. (2) (*cf.* [15]):

$$f_n = f \cdot (1 - \cos(\pi/2 - \delta)) \tag{2}$$

To obtain the two edges of the reflector for any day, the following equation is used:

$$(x_{1,2})_n = 2 \cdot f_n \cdot \tan(\alpha + \delta/2) \pm \sqrt{\frac{A_s c}{\pi \cdot \cos(\alpha)}} \cdot \cos(\alpha + \delta_n/2) \tag{3}$$

The mirror's positions and aiming points vectors are then obtained by deriving the shape of the parabola.

Subsequently, the parabola is rotated along three different axes to be representative of the exact position on Earth and the exact time.

To change from the general coordinate system "O = focal point", "positive x = towards South", "positive y = towards East" and "positive z = towards zenith" to the local coordinate system corresponding to a paraboloid with the Sun at its exact position and parameterized with (x^*, y^*, z^*), three successive rotations are performed: one for the declination, then one for the hour angle and finally one for the latitude. When using an actual reflector, these three rotations can be performed with some errors, respectively called ϵ_δ, ϵ_ω and ϵ_{lat}. The two former can be converted in delays of daily adjustment in days and tracking adjustment in minutes; the latter is an error in the inclination of the parabola and can be therefore given in degrees. One final rotation is performed in the global coordinate system to represent a potential error in the adjustment of the North–South alignment of the parabola and is called ϵ_{South} (in degrees). The coordinate of a mirror facet in the main coordinate system with respect to its coordinates in the local system is therefore given by:

$$\begin{pmatrix} x \\ y \\ z \end{pmatrix} = R_z(\epsilon_{South}) \cdot R_y(-lat - \epsilon_{lat}) \cdot R_x(-\omega - \epsilon_\omega) \cdot R_y(\delta + \epsilon_\delta) \cdot \begin{pmatrix} x^* \\ y^* \\ z^* \end{pmatrix} \tag{4}$$

where $R_i(\theta)$ is the rotation matrix around the local axis e_i and with an angle θ.

The receiver is located and centered at the focal point. It is generally stated that its inclination angle β should correspond to the latitude in order to face towards the rotation line that is almost at the center of the reflector. To evaluate the magnitude of the impact of a wrong adjustment of the receiver, errors on its horizontal position, ϵ_{dist}, and on its inclination, ϵ_β, will also be considered. The receiver's global position and aiming vector are therefore given by:

$$\begin{pmatrix} x_R \\ y_R \\ z_R \end{pmatrix} = \begin{pmatrix} 0 - \epsilon_{dist} \cdot cos(\epsilon_{South}) \\ 0 + \epsilon_{dist} \cdot sin(\epsilon_{South}) \\ 0 \end{pmatrix} \tag{5}$$

$$\begin{pmatrix} x_{aim_R} \\ y_{aim_R} \\ z_{aim_R} \end{pmatrix} = \begin{pmatrix} cos(\beta + \epsilon_\beta) \cdot cos(\epsilon_{South}) \\ cos(\beta + \epsilon_\beta) \cdot sin(\epsilon_{South}) \\ sin(\beta + \epsilon_\beta) \end{pmatrix} \tag{6}$$

To sum up, six different adjustment errors will be evaluated: *i.e.* ϵ_{lat}, ϵ_{South}, ϵ_δ, ϵ_ω, ϵ_β and ϵ_{dist}. Some of these errors are represented on Fig. 1, while ϵ_ω and ϵ_{South} are in a perpendicular plane and would necessitate a view from above to be pictured.

2.3. Optical errors of the system

The concentration factor of the Scheffler reflector depends first on its size and focal distance [15], *i.e.* the higher the view factor of the parabola from the receiver, the higher the possible concentration. These parameters are fixed when designing the system. It also strongly depends on the optical errors of the whole system. The total optical error σ_{tot} can be estimated with Eq. (7) [29] and depends on five parameters:

- the angular apparent radius of the Sun $\theta_{sun} = 4.65$ mrad;
- the quality of the specular reflection of the mirrors, quantified in Soltrace by the "specularity error" σ_{spec}. In this case, it depends on the quality of the mirrors, knowing that a glass mirror creates two refractions before and after the reflection on the metal coating, and that a mirror can be dirty and scratched;
- the deviation of the local curvature of the parabola from its theoretical shape, quantified in Soltrace by the "slope error" σ_{slope}. In this case, this error depends directly on the chosen size of the square flat mirrors;
- the deviation of the parabola from its theoretical shape, generally quantified by an error σ_{shape} that is independent from σ_{slope}. If the position of the facets is correctly chosen, this error is null in the numerical model. In an actual Scheffler reflector, it can be very important because it represents its ability to reproduce the theoretical shape by bending;
- the deviation between the aiming point of the parabola and the actual position of the Sun, represented by a tracking error $\sigma_{tracking}$.

$$\sigma_{tot}^2 = \sigma_{sun}^2 + \sigma_{spec}^2 + 4 \cdot \sigma_{slope}^2 + 4 \cdot \sigma_{shape}^2 + \sigma_{tracking}^2 \tag{7}$$

In Soltrace, the shape errors are implicitly created when designing the different optical stages (position, orientation) and therefore, they cannot be specified by users. The tracking errors can be easily created by users when defining the system. While the angular size of the Sun in the sky is well known, the coupling between the specularity and slope errors is difficult to evaluate without their experimental characterization by photogrammetry [30] or deflectometry [31]. As a consequence, one way to artificially increase the total error σ_{tot} is to multiply the size of the Sun with an arbitrary factor k_{sun}. This method has no physical significance but leads to similar focal image than using errors while preventing a wrong prediction of their values. In this work, the k_{sun} factor will be varied in order to both fit experimental results and observe its combined influence with other experimental errors (positions and angles).

2.4. Chosen input parameters

In this work, the modeled reflector is fitted to an experimental set-up in Marseille, France, and has the following features: $f = 1.43$ m, $lat = 43.345°$, $A_{sc} = 8$ m^2 and $\alpha = 43.23°$. The Scheffler reflector is composed of small mirror facets of 0.1 m × 0.1 m. The characteristics of the receiver are chosen so as to limit its influence on the results (large size, perfect absorption). The target is therefore a flat square with an arbitrary surface of 1 m^2, centered at the parabola focal point and more or less inclined towards the reflector. A real receiver would be at the same position and would have a different shape and size, *e.g.* a disk with a 26 cm diameter.

The general optical parameters are the following:

- slope and specularity errors are set to 0.001 mrad and are Gaussian;
- the reflectivity of mirrors is set to 90% while the target's is set to 0%. Transmittivity is always 0%. Absorptivity of the target is set to 100%;
- the Sun is initially modeled as a pillbox with an angular apparent radius of 4.65 mrad; This value can be multiplied by k_{sun} to represent the total optical errors. The DNI is 900 W m^{-2}.

2.5. Processing of results

Power density maps are computed using the local coordinate system of the receiver, parameterized with (x^*, y^*). They highly depend on the pixel sizes that are changing from one result to the other. Therefore, no comparison should be made between two figures, except when it is forced to the same value.

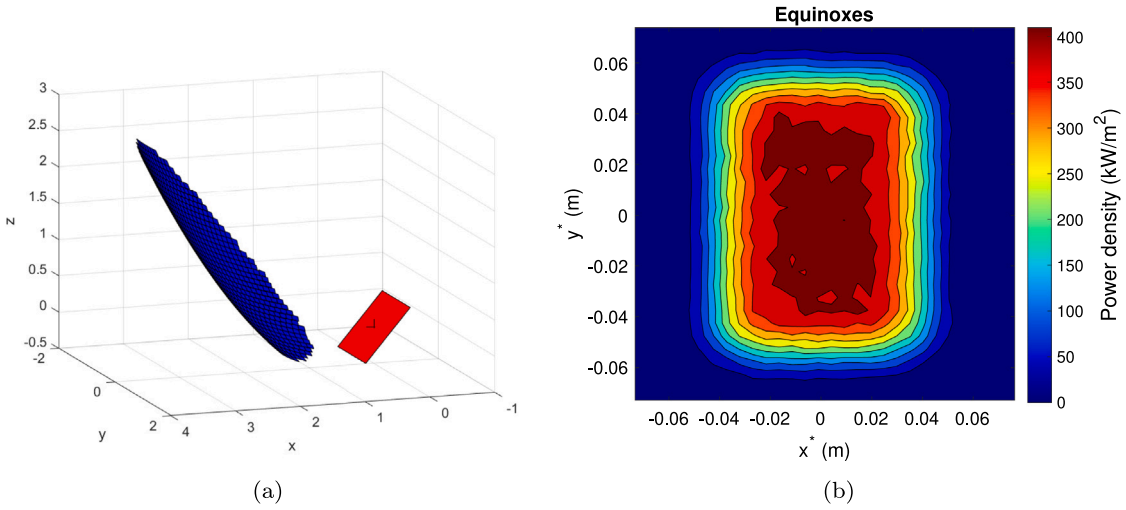

Fig. 3. Reflector's shape (and inclined plane receiver) for the equinox in Marseille ($lat = 43°$, $long = 1°$) with mirror facets accommodating the parabola's shape ($A_{ap} = 5.85$ m^2) (a). Focal image that is obtained from this parabola, with no further optical error (b).

2.6. Key quantities for the analysis

In this study, several simulations were performed:

- one reference case consisting in a parabola with facets whose positions follow the theoretical shape;
- parametric studies on the total optical error of this parabola to find a possible configuration for the actual experimental results that are used as tuning reference;
- a parametric study on the tilt of the receiver/target, the accuracy of the Sun's tracking and on the parabola's shape and position in order to understand the possible flexibilities of the Scheffler system.

Results will focus on power density distribution and average power density $\langle\phi\rangle$ received by the target, *c.f.* Eq. (8), defined as the ratio between the total incident power P_{tot} (see Eq. (9)) and the image total area A_{im}.

$$\langle\phi\rangle = \frac{P_{tot}}{A_{im}} \tag{8}$$

$$P_{tot} = A_{ap} \cdot DNI \cdot \rho_{mirrors} \tag{9}$$

A_{im} is defined as the area circling all the rays that are hitting the target while its centroid is defined as the average position of the rays in the target's local reference frame. When the optical and position errors are not too important, all the rays are hitting the target and both the impacted area and the centroid position can be estimated. For very important errors, some rays miss the target. Concentration ratio can be defined with respect to power density *v.s.* DNI and reflectivity of mirrors $\rho_{mirrors}$, or with aperture area of the reflector A_{ap} *v.s.* the image surface area A_{im}.

$$CR = \frac{A_{ap}}{A_{im}} = \frac{\langle\phi\rangle}{DNI \cdot \rho_{mirrors}} \tag{10}$$

It should be noted that since Soltrace is based on statistics, it is likely that a solitary ray deviates significantly from the others and substantially increases the total calculated area. The last indicator will therefore be P_{rec}, the total power that reaches a hypothetical 26 cm diameter disk receiver located in (0, 0, 0). In the ideal conditions that represents former experimental results (*vide infra*), this disk receives 95% of the power that is reflected by the parabola. In non-ideal conditions, this power received by this hypothetical receiver will serve as criterion for error quantification. Note that all powers do not take into account the capacity of the receiver to absorb them, *i.e.* only the incoming power value and distribution will be discussed.

3. Results and discussion

3.1. Model of a Scheffler reflector with facets and no further optical errors

A "perfect" Scheffler reflector would use a flexible and continuous mirror with no optical errors and would give its maximum concentration ratio. Such reflector has been modeled, see Appendix B.1, but it is not enough versatile and ergonomic to be used as the main model. Using 0.1 m × 0.1 m flat facets, as illustrated in 3-a, inherently creates optical aberrations resulting in focal images that are larger than the ones that could be obtained with continuous parabolas. On Fig. 3-b, it can be observed that because of the facets and with no further optical errors, the size of the focal image is limited by the size of the facets (0.1 m × 0.1 m) and gives an image with a rectangular shape. The system gives an average power density of 233.5 kW m^{-2} for 100% of P_{tot} and 427.1 kW m^{-2} for 95% of P_{tot}, *i.e.* focal image areas of 0.0203 m^2 and 0.0111.0 m^2, respectively. It corresponds to CR of 288 or 527, respectively.

These areas are largely lower than the actual focal images obtained from experimental results with facets, *i.e.* 0.113 m^2 and 0.053 m^2, respectively [21]. Therefore, further optical errors have to be implemented in the simulations.

3.2. Model of a Scheffler reflector with mirror facets and optical errors so as to obtain "experimental-like" results

The influence of the multiplicator k_{sun} on the average power density $\langle\phi\rangle$ and on the centroid position is pictured in Fig. 4.

The objective was to find the k_{sun} value giving the best fitting with experimental data [21]. The comparison between the experimental and the numerical Gaussian curves showed that $k_{sun} = 7.2$ provides the best results. Fig. 5 shows the comparison between the predicted focal image of the Sun with the best fitting value and the experimental focal image that was presented in [21]. For this comparison, the pixel size is the same for numerical and experimental results, therefore both the power distributions and absolute values can be compared.

The results are in good agreement, with 95% of the 2.6 kW total power received by a disk with a 26 cm diameter. However, the uncertainty is very large because of all the experimental assumptions that were made here; we estimate that this kind of Scheffler reflector can be correctly simulated with $k_{sun} = 7 \pm 2$. Thanks to the comparison with another model with a continuous parabola, it is possible to roughly estimate the total error to 15–25 mrad (see Appendix B for details).

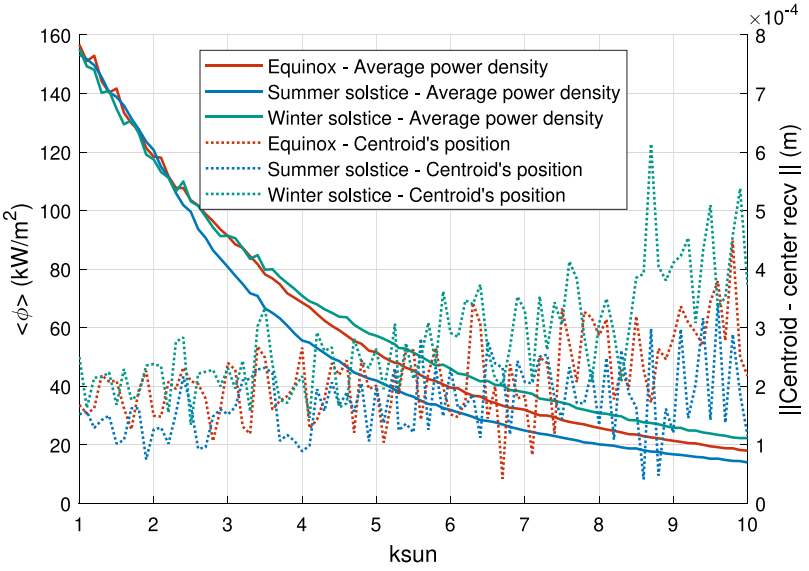

Fig. 4. Influence of the Sun multiplicator k_{sun} on the average power density and the centroid's position.

3.3. Variations of the focal image with day and time

Because some geometric parameters change with day and time, *e.g.* the theoretical shape of the parabola, the distance and view angles of its edge with respect to the focal point, etc., the theoretical focal image should vary accordingly. Besides, when bending the reflector in the vertical direction with the two integrated extensible arms, a possible horizontal deformation of the reflector can occur, resulting in distortion of the obtained images [20]. Previous studies theoretically predicted or experimentally found that the focal image size and shape changes with respect to the day and time. For instance, Reddy et al. [15] found that the focal image should be larger and more elliptical for the summer solstice than for the winter solstice. This result was also confirmed by the experimental work of Dib [22] but not by our previous experimental work (some variations were observed but no seasonal trend was shown [21]). More experimental results on various Scheffler reflectors are needed to conclude. Meanwhile, numerical studies with possible k_{sun} give an idea of the possible variations that can be expected. For instance, Fig. 6 shows the power density maps received by an inclined receiver that were obtained with $k_{sun} = 7$ for the solar noons of the equinox, the summer solstice and the winter solstice. The only visible difference between the figures is the total power that is dependent on the daily aperture of the reflector; the apparent sizes are very similar. Different times of the day were also simulated and the results show no difference because the power density map is more or less a 2D-Gaussian function rotating around its center. Concentration factors are also considerably lower than in [15], *i.e.* in the range of 31–46, or 58–87 if the 26 cm virtual disk is used as receiver, against 1000–7000. This is because actual optical errors are tremendously high.

It can be concluded that, because the optical errors are more important than the theoretical geometric variations, the shape of the focal image is almost always circular and the important variations that could be observed for a perfect shape are negligible when a realistic case is used.

The same results for $k_{sun} = 1$ are given in Appendix C.1 and variations between seasons are more visible.

The importance of the experimental optical errors of actual Scheffler parabolas motivated the parametric studies that follows. With the developed model and the knowledge from experimental results, it is possible to assess the room for maneuver when positioning and using such solar reflectors.

3.4. Sensibility analysis to set-up defects and implications for the model

When positioning a Scheffler reflector, the user should (see Fig. 1):

- align the reflector with the North–South axis, towards South in the Northern hemisphere, and towards North in the Southern hemisphere;
- incline the reflector in order to get the rotation axis parallel to the Earth's rotation axis, *i.e.* an inclination to the latitude with respect to the ground;
- position the receiver exactly where the focal point/image should be;
- incline the receiver to an angle close to the latitude;
- bend the parabola in order to obtain the exact shape for the day of the experiment;
- turn the parabola's rotating axis in order to track the Sun.

All these steps will be performed with some errors. The following parametric study aims to give the error margin that is acceptable to obtain satisfying results. The chosen criterions can be (i) the average solar power density arriving onto a target (arbitrarily defined as a 1 m × 1 m plane inclined to the latitude and centered at the focal point), given by Eq. (8), (ii) the position of the centroid of the focal image in the receiver, (iii) the total power arriving onto a 26 cm diameter disk located in (0, 0, 0) and representing a potential receiver. These criterions evaluate how the focal image is growing and/or moving, *i.e.* how it can go out of the potential receiver. In the following results, we consider a single error to be acceptable if it results in a reduction of less than 10% in the average power density over the 26 cm disk surface on the day most sensitive to the chosen parameter. Other parameters will be given as complementary information. Results will be given for a reflector located in Marseille, for the equinox and the two solstices. As optical errors plays an important role in the dependence of the results to the different design errors, the same parametric study has been performed for k_{sun} of 1, 3, 5, 7 and 9. Results with $k_{sun} = 7$ will be discussed in the following sections while others are provided in Appendices C.1–C.4 and obviously show that margin for error is weakened when k_{sun} decreases.

3.4.1. Horizontal alignment of the scheffler reflector

With $k_{sun} = 7$, Fig. 7-a shows the consequences of an incorrect southward positioning of the reflector on the total power P_{rec} received

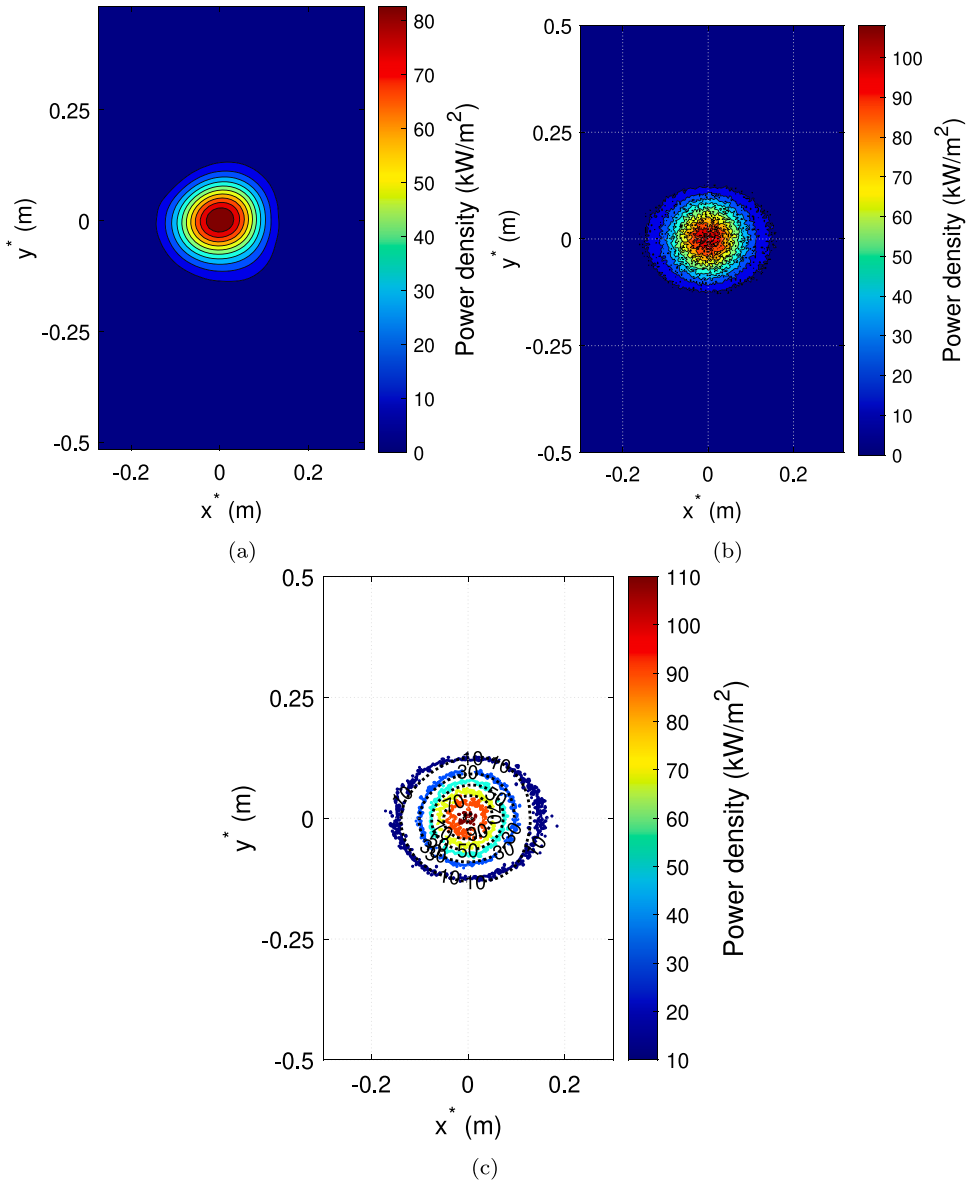

Fig. 5. Comparison between the experimental results from a 8 m^2 Scheffler reflector (14 of June 2022, Marseille, 12 p.m solar time solar, DNI = 900 W m^{-2}) (a) and the numerical results with the best fitting k_{sun} and the same bining (bining = 3.5 × 3.5 mm^2) (b). Comparison of the iso-power-density lines (c).

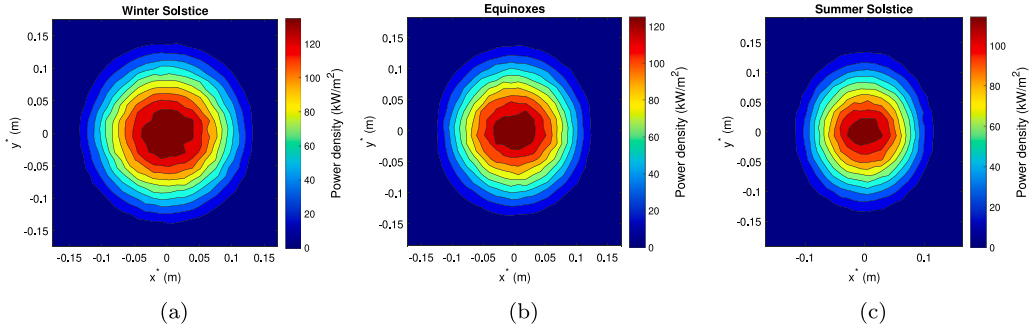

Fig. 6. Variation of the numerical focal image with the declination for k_{sun} = 7: Winter solstice - P_{tot} = 5.88 kW (a), Spring equinox - P_{tot} = 4.94 kW (b) and Summer solstice - P_{tot} = 3.87 kW (c).

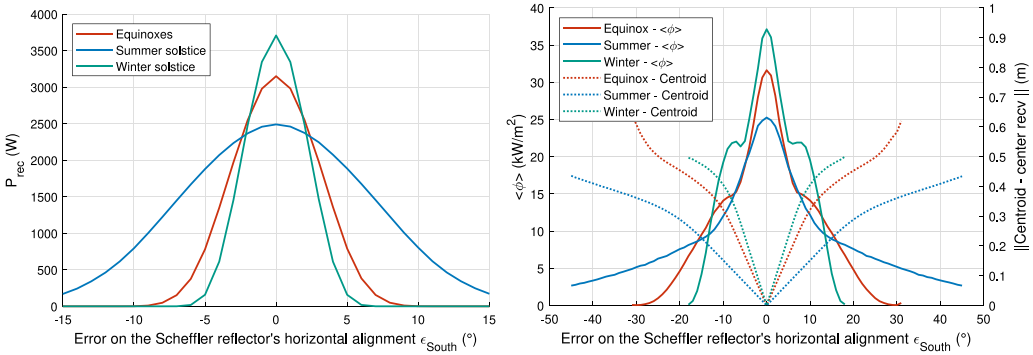

Fig. 7. With $k_{sun} = 7$, theoretical effects of a wrong North–South alignment of a Scheffler reflector on the power received by a hypothetical disk receiver with a diameter of 26 cm (a); on the position and power density of the whole focal image (1 m × 1 m plane target) (b).

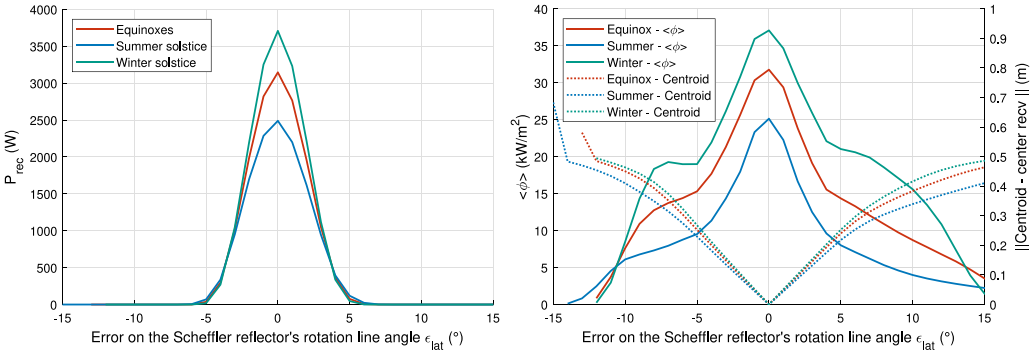

(a) (b)

Fig. 8. With $k_{sun} = 7$, theoretical effects of a wrong inclination of the Scheffler reflector's axis of rotation on the power received by a hypothetical disk receiver with a diameter of 26 cm (a); on the position and power density of the whole focal image (1 m × 1 m plane target) (b).

by the 26 cm diameter virtual receiver. Fig. 7-b shows the impact of this same parameter on the average power received by the 1 m^2 target and on the centroid position. Performance appears to be highly sensitive to this parameter, with a 1° error leading to a 10% reduction in P_{rec} for the winter equinox (the most sensitive day) and an image shift of up to 4.6 cm. The impact on the average power density of the target is smaller, and its changes in slope for errors of around ±5° are due to the fact that the rays start to miss the 1 m^2 target. The North–South alignment of the dish is therefore of paramount importance, and must be conscientiously set to an accuracy of 1°; a compass is insufficient due to the Earth's magnetic declination.

3.4.2. Rotation axis' angle with respect to the ground

The angle of the axis of rotation in relation to the ground must be set to be equal to the latitude of the location. Depending on the tools used for this adjustment, errors may be created. Fig. 8-a shows that this error can be as much as 0.8° to accommodate a 10% decrease in P_{rec}, resulting in a focal image shift of around 4.0 cm (for $k_{sun} = 7$). This inclination is therefore also an important parameter, although being easy to adjust using a digital level. Note that the power density behavior of the focal image is not exactly symmetrical with respect to the shift of the line of rotation, due to the change of aperture area of the reflector.

3.4.3. Horizontal position of the receiver

Fig. 9 shows the consequences of incorrect horizontal positioning of the receiver, *i.e.* placing it too close or too far from the Scheffler reflector, with $k_{sun} = 7$. According to the results, a maximum error of 6 cm is tolerated to avoid a too great reduction in the power received by the virtual disk. This results in a 3 cm shift in the focal image and a 10% reduction in power for the winter solstice results, which are once again the most affected by this parameter.

3.4.4. Tilt of the receiver

The variation in power density and centroid position as a function of receiver inclination and with $k_{sun} = 7$ is shown in Fig. 10-b. It can be seen from this figure that placing the receiver vertically does not change the centroid position, but spreads out some of the Sun's rays, resulting in a sharp drop in the average power density on the target. However, most of the power still reaches the hypothetical receiver (see Fig. 10-a): a 10% reduction in P_{rec} corresponds to a 31° error in inclination (*i.e.* 74° instead of 43°), whereas positioning the receiver vertically modifies it by only 12 %. As a conclusion, while it is advised to tilt the receiver according to latitude, having a vertical receiver such as in our experimental work [21], is not very detrimental to the reflector's performance. Besides, it does not seem that inclining by the latitude angle is exactly the best compromise: the average power density also depends on the distance between the focal point and the two edges of the reflector that are different from one season to the other.

3.4.5. Declination adjustment

Scheffler reflectors need to be adjusted regularly, using integrated extensible arms that bend the reflector into a given parabolic shape. The question arises as to how often this adjustment is necessary. Fig. 11 shows that, with $k_{sun} = 7$, it is sufficient to adjust the shape of the parabola every 16 days near the solstices, but only every two days near the equinoxes. This is because the Sun's declination changes much more rapidly for the latter (the derivative of the declination is 0 for the solstices and maximum for the equinoxes). However, when the 10% decrease in P_{rec} is observed, the focal point may have moved 4 cm from its initial point.

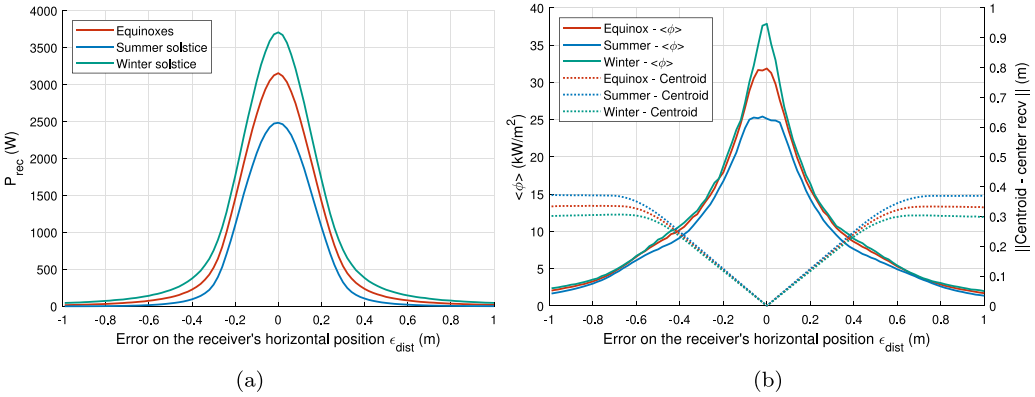

(a) (b)

Fig. 9. With $k_{sun} = 7$, theoretical effects of a wrong horizontal position of the Scheffler's receiver (inclined with the latitude to face the center of the parabola) on the power received by a hypothetical disk receiver with a diameter of 26 cm (a) and on the position and power density of the whole focal image (1 m × 1 m plane target) (b).

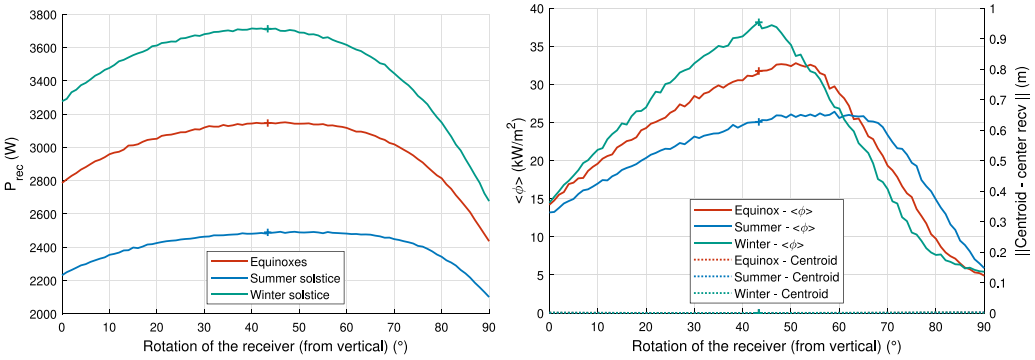

Fig. 10. With $k_{sun} = 7$, theoretical effects of a wrong inclination (from vertical) of the Scheffler's receiver (best position would be an inclination angle equal to the latitude, marked by '+' signs here) on the power received by a hypothetical disk receiver with a diameter of 26 cm (a) and on the position and power density of the whole focal image (1 m × 1 m plane target) (b).

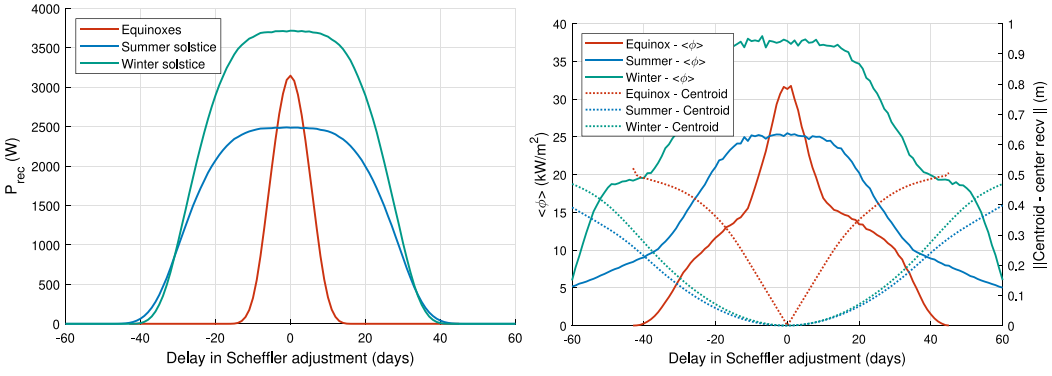

(a) (b)

Fig. 11. With $k_{sun} = 7$, theoretical effects of a delay in days in the tuning of the Scheffler reflector's curvature on the power received by a hypothetical disk receiver with a diameter of 26 cm (a) and on the position and power density of the whole focal image (1 m × 1 m plane target) (b).

3.4.6. Tracking error

With $k_{sun} = 7$, Fig. 12 shows whether the Scheffler parabola should follow the Sun with a very precise tracking system. The criterion is met if the tracking system has a delay of less than 4 min, resulting in a reduction in P_{rec} of 10% and a shift of the focal image of 4.6 cm, for the winter solstice. This can easily be achieved using an automatic device or a pendulum.

3.4.7. Combination of errors and discussions

In a real experimental device, setting and positioning errors can occur simultaneously. In fact, Scheffler reflectors do not benefit from the same care as regular CSP systems: they are usually positioned and adjusted manually, with simple tools, explaining multiple errors. Fig. 13 shows the obtained focal images for $A_{sc} = 8$ m^2, $f = 1.43$ m, $k_{sun} = 7$ and if all the previous errors are set to their maximum

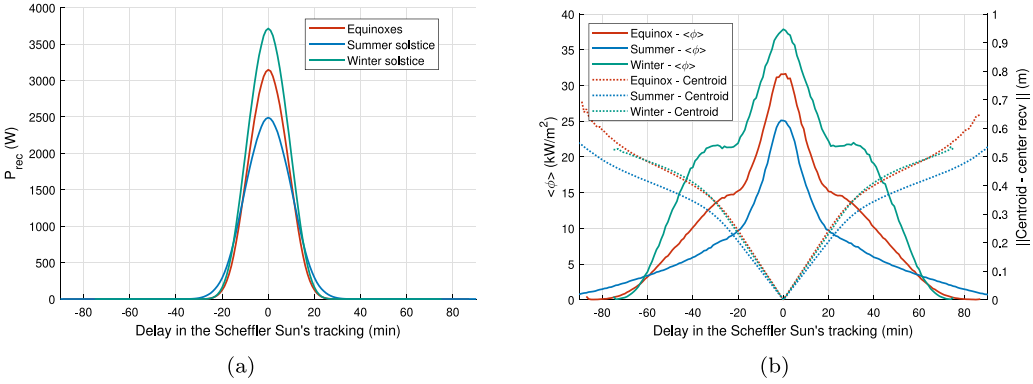

Fig. 12. With $k_{sun} = 7$, theoretical effects of a delay in minutes in the tracking system of the Scheffler reflector on: the power received by a hypothetical disk receiver with a diameter of 26 cm (a) and on the position and power density of the whole focal image (1 m × 1 m plane target) (b).

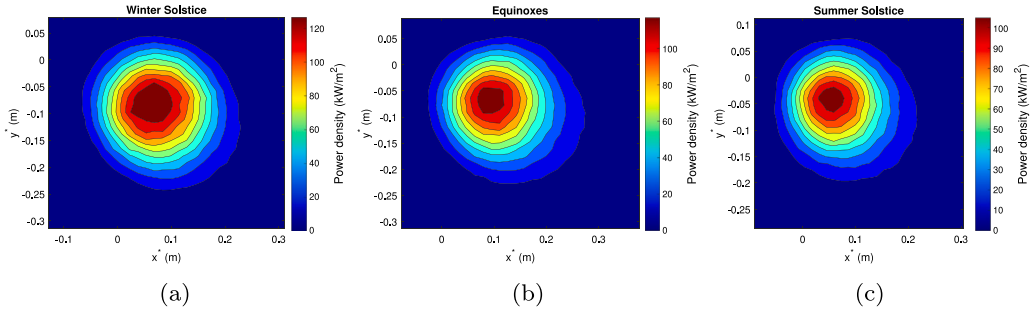

Fig. 13. Obtained focal images with $k_{sun} = 7$ when all the threshold errors are put simultaneously, for winter solstice (a), equinox (b) and summer solstice (c).

values which have been defined, *i.e.* a North–South alignment error of 1°, a rotation axis error of 0.8°, an error of 6 cm on the horizontal position of the receiver, a declination adjustment error corresponding to 2 days, tracking error corresponding to 4 min, and a receiver with an inclination of 74°. Results can be compared to those shown in Fig. 6. While the image is a lot distorted, the concentration is still acceptable. However, it is displaced from the focal point (0, 0) and therefore misses the virtual target. The calculated P_{rec} are 1.82 kW, 1.64 kW and 1.19 kW, for the winter solstice, the summer solstice and the spring equinox, respectively. It corresponds to power reductions of 69%, 67% and 69% when compared to the case with no error. This is obviously not acceptable.

In order to better assess the influence of each parameter as well as their interactions on system performance, sensitivity studies were carried out. The methodology is similar to the one used in [32,33] and it was applied to one case with $k_{sun} = 1$ and one with $k_{sun} = 7$. These analyses were conducted using a 2^N factorial design of experiments [34], where N represents the number of parameters x_i. Each parameter takes two values (minimum and maximum) selected from a reference value ($mean(x_i) = x_{ref}$). This method quantifies the effects of parameters and their interactions on a specific output objective y. The fundamental concept involves approximating the system response as a function of the normalized parameters or input factors X_i:

$$y = \beta_0 + \sum_{i_1=1}^{N} \beta_{i_1} X_{i_1} + \sum_{i_1=1}^{N} \sum_{i_2>i_1}^{N} \beta_{i_1 i_2} X_{i_1} X_{i_2} + \sum_{i_1=1}^{N} \sum_{i_1>i_2}^{N} \sum_{i_3>i_2}^{N} \beta_{i_1 i_2 i_3} X_{i_1} X_{i_2} X_{i_3} + \cdots + \beta_{i_1 i_2 \ldots i_N} X_{i_1} X_{i_2} \ldots X_{i_N} \quad (11)$$

$$X_i = \frac{x_i - x_{i_{ref}}}{(max(x_i) - min(x_i))/2}, \text{ i=1,N} \quad (12)$$

where the subscript $_{ref}$ denotes the reference case. The different effects $\hat{\beta} = \beta_0, \beta_{i_1}, \beta_{i_1 i_2}, \ldots, \beta_{i_1 i_2 \ldots i_N}$ are obtained by solving the linear system described in Eq. (11). β_0 can be calculated with the mean value of the output objective y calculated for all parameter sets.

The sum of squares SS for different effects indicates the percentage contribution of each model term relative to the total sum of squares SST:

$$SS_i = 2^N \beta_i{}^2, \; i = 1, 2^N - 1 \quad (13)$$

$$SST = \sum_{i=1}^{2^N - 1} SS_i = \sum_{i=1}^{2^N} y_i^2 - \frac{(\sum_{i=1}^{2^N} y_i)^2}{2^N} \quad (14)$$

where y_i with $i = \{1, \ldots, 2^N\}$ are the different output quantities from 2^N simulations. For more details on the method, see the relevant literature, *e.g.* [32,33]. The quantity considered in the following is the average power density $\langle\phi\rangle$.

In our study, $N = 5$ input parameters of the model are considered:

- d = ϵ_{dist} (m), d1 = delay in Scheffler adjustment (days);
- d2 = delay in the Scheffler Sun's tracking (min);
- S = ϵ_{South}(°);
- R = ϵ_{lat}(°).

Table 1 summarizes the chosen ranges for the parameters considered by the sensitivity study. Fig. 14 shows the sensitivity of $\langle\phi\rangle$ to both individual parameters and their combinations for the two values of k_{sun}.

The interaction effects (d1d2), *i.e* between the delay in Scheffler adjustment and the delay in the Scheffler Sun's tracking, dominates the process. It accounts for ~87% and ~70% of the total variability, respectively with $k_{sun} = 1$ and $k_{sun} = 7$. This demonstrates the importance of paying close attention to these two setting parameters, even if their individual contribution is negligible.

The effect due to the combination between the error on the receiver's horizontal position and the error on the Scheffler reflector's rotation line angle, (dR), is still significant but with much less importance with ~7% of the total variability with $k_{sun} = 1$. With $k_{sun} = 7$, the

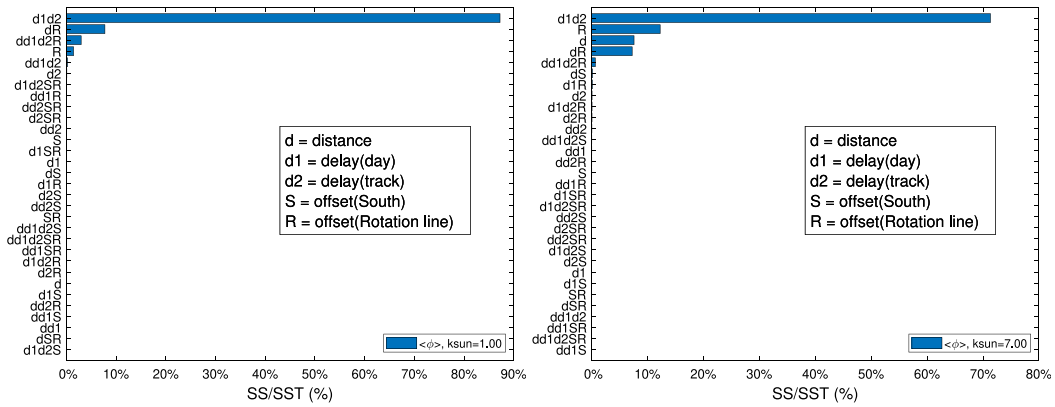

Fig. 14. Normalized sum of squares SS/SST with $ksun = 1$ (a) and $ksun = 7$ (b).

Table 1
Parameter levels for the sensitivity study with $N = 5$ parameters.

x_i	Reference	min	max
d = ϵ_{dist} (m)	0	−0.06	0.06
d1 = Delay in Scheffler adjustment (days)	0	−2	2
d2 = Delay in the Scheffler Sun's tracking (min)	0	−4	4
S = ϵ_{South}(°)	0	−1	1
R = ϵ_{lat}(°)	0	−0.8	0.8

influence of the angle of the axis of rotation of the Scheffler reflector is the second most important factor, with ∼12%. This parameter ranks fourth with $k_{sun} = 1$ with ∼1.5% of the total variability. Moreover, the interaction between the four parameters (dd1d2R) is less significant with $k_{sun} = 7$ than with $k_{sun} = 1$. The sensitivity study shows that the error on the Scheffler reflector's horizontal alignment (S) has no influence on the combined results. The latter results were expected, since the receiver's position is adapted to this alignment, which is not the case for the other parameters. Finally, we note that with $k_{sun} = 7$, the individual distance error parameter (d) has little influence, whereas it has none with $k_{sun} = 1$.

Considering the values of SST ($SST(k_{sun} = 1) \sim 2418$ (kW m^{-2})^2 and $SST(k_{sun} = 7) \sim 69.4$ (kW m^{-2})^2), the system is less sensitive at stronger optical errors, corresponding to increasing k_{sun}, i.e. optical errors make the system more tolerant to other types of error.

It should be noted that the experimental set-up that has been used to calibrate the model with *a priori* no error gave results that were actually dependent on adjustment errors. We estimate that the reflector's south positioning was made with a compass to an accuracy of about 3°; the rotation axis is inclined with a numerical level, to an accuracy of about 2°, the declination is adjusted by hand every day, with an unknown accuracy (∼7 days), the tracking system is automatic, with an accuracy of 1.25° (5 min) and the receiver is put at the focal point with an horizontal accuracy of ∼5 cm. If we simulate the parabola with all those errors and with $k_{sun} = 7$, the results are also catastrophic. Several conclusions can be drawn from these previous results: (i) the experimental errors that were obtained when manually adjusting the reflector are necessarily lower than both the chosen limits and the estimated accuracies; (ii) since the declination adjustment is manual and depends on qualitative results (*i.e.* the reflector is inclined and bent until the focal image is centered on the receiver and small enough to be satisfying), we strongly believe that users compensate part of the errors when they change the curvature of the parabola; (iii) since errors are not separable and can compensate each other, assuming reference case with only one parameter (k_{sun}) to represent all the errors can give good order of magnitudes on their relative influences.

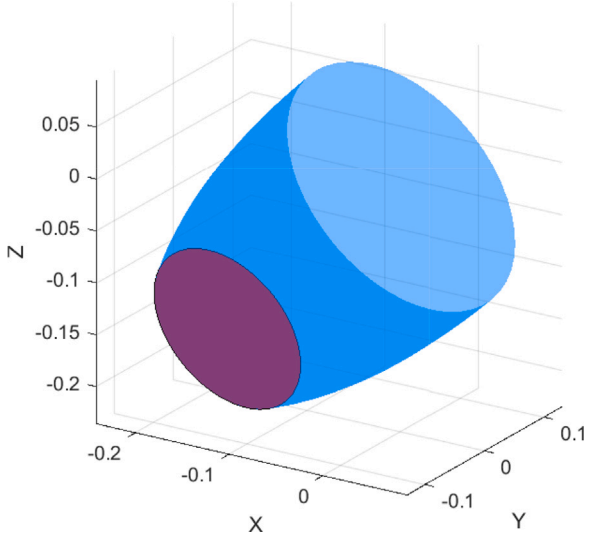

Fig. 15. The designed 3D-CPC (in blue) with a 26 cm entrance diameter that increases the concentration of the Scheffler-based solar concentrator, and the new disk receiver (16 cm diameter) in purple.

3.5. Design of a secondary optics in order to maximize concentration

The present model can be used to design and simulate the performance of a Scheffler reflector associated with a secondary optical system. For example, to increase the system's concentration ratio, a suitable compound parabolic collector (CPC) can be designed, following [35]. In the present example, we have chosen to design a 3D CPC whose entrance aperture is centered on (0, 0, 0) and faces the central point of the Scheffler reflector. The secondary reflector therefore has an angle of inclination equal to the latitude of the location. Depending on the angle of view of the Scheffler reflector from (0, 0, 0), and according to various simulations, the best compromise is a design with an acceptance angle of 40°, an entrance diameter of 26.0 cm, an exit diameter of 16.7 cm and a length of 25.4 cm, see Fig. 15.

Maps of the power density distributions reaching a circular receiver located at the output of the CPC's secondary reflector are given in Fig. 16. If we compare them with those in Fig. 6, we can see that while total power has not changed much (only some losses due to imperfect reflections in the secondary reflector, *i.e.* a reflectivity of 90 %), average power densities have increased from 47 kW m^{-2} - 71 kW m^{-2} on the previous 26 cm diameter disk receiver to 156 kW m^{-2} - 222 kW m^{-2} on the new 16.7 cm disk receiver. This involves a multiplication factor

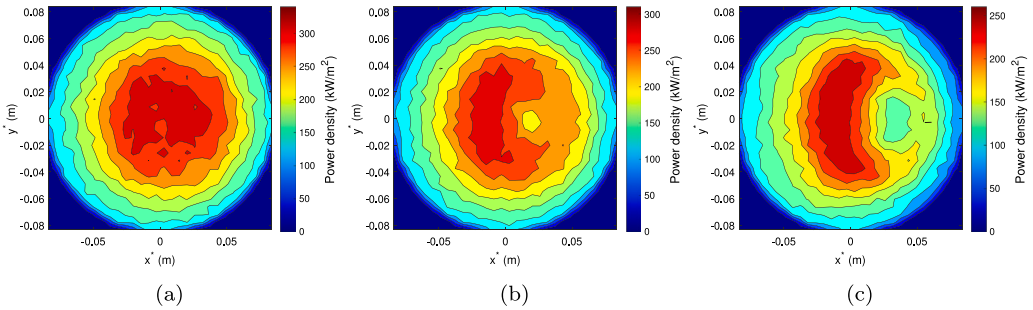

Fig. 16. Variations of the numerical focal image with the declination with $k_{sun} = 7$ and when a 3D-CPC secondary reflector (entrance diameter: 26 cm, exit diameter: 16.7 cm, reflectivity: 90%) is used: Winter solstice - $P_{tot} = 4.86$ kW (a), Equinoxes - $P_{tot} = 4.26$ kW (b) and Summer solstice - $P_{tot} = 3.41$ kW; ($DNI = 900$ W m^{-2}) (c).

of 3.3, with maximum local power densities of up to 337 kW m^{-2} vs. 120 kW m^{-2} without the CPC.

4. Conclusion

The present work shares an open-language and versatile model of a Scheffler reflector enabling Monte-Carlo-Ray-Tracing simulation with the Soltrace software. This model is able to take into account the location, the solar time, the Scheffler reflector's characteristics, the geometry of the receiver, and the tracking and positioning errors. The objective of this model is to help users to understand and build new reflectors, but also to provide a tool simplifying the design of new secondary optical systems that could increase the performance of the solar concentrating system. The main results of this study are:

- Experimental set-up using Scheffler reflectors have huge optical errors that should be lowered.
- The seasonal variations that are predicted by the theory are not visible when considering an actual Scheffler reflector, *i.e.* with realistic optical errors. The influence of the latter hides the influence of the former.
- While positioning a reflector, doing the adjustments and tracking the Sun is not an easy task, we showed that error margins are 1° for the North–South alignment, 0.8° for the rotation axis inclination, 6 cm for the horizontal position of the receiver, 2 days for the declination adjustment and 4 minutes for the tracking system. All those errors taken independently lead to 10 % reduction of the total power received by a hypothetical disk receiver with a diameter of 26 cm. The inclination of the receiver has lower influence on the results, with only a 12 % decrease of the power when putting vertically instead of following the latitude. The given results are for an 8 m^2 reflector with a focal distance of 1.43 m and located in Marseille ($lat. 43°$ N), however the model can be used to predict any other configuration (other size, other focal distance, lying reflectors, etc.).
- When taking all the previous errors together, performance tend to decrease by ≈ 69 % and sensitivity analysis demonstrated that the interactions between daily adjustment error ϵ_δ and tracking error ϵ_ω dominates the set of positioning and adjustment errors.
- In case of Scheffler reflector with better tuning or reflector, results were also given for other optical errors. Obviously, the better the optics, the smaller are the error margins.
- By using appropriate secondary optics, for instance non-imaging optics such as 3D-CPC reflectors, power densities can be multiplied by 3.3.

Following works should include : (i) full optical characterization of Scheffler reflectors in order to quantify the distribution of their optical losses, whether being slope, specularity or shape, to eventually reduce their values; (ii) the design of secondary optics for Scheffler reflectors and adapted to the various needs of the users.

Fundings

This work was supported by the Region Provence-Alpes-Côte d'Azur and the company Le Présage as part of the "Emplois Jeunes Doctorants" scheme, France. It was also supported by the Institute of Mechanics and Engineering of Aix-Marseille University. This work received support from the french government under the France 2030 investment plan, France, as part of the Initiative d'Excellence d'Aix-Marseille Université AMX-20-TRA-034. None of these funding sources were involved in study design; in the collection, analysis and interpretation of data; in the writing of the report; and in the decision to submit the article for publication.

CRediT authorship contribution statement

Thomas Fasquelle: Writing – review & editing, Writing – original draft, Visualization, Software, Project administration, Methodology, Investigation, Funding acquisition, Formal analysis, Conceptualization. **Benjamin Kadoch:** Writing – review & editing, Visualization, Validation, Software, Project administration, Investigation, Funding acquisition, Formal analysis, Conceptualization. **Gabriel Guillet:** Writing – review & editing, Visualization, Conceptualization. **Séverine Barbosa:** Writing – review & editing, Project administration, Funding acquisition, Conceptualization.

Declaration of competing interest

The authors declare that they have no known competing financial interests or personal relationships that could have appeared to influence the work reported in this paper.

Acknowledgments

We would like to thank professor Manuel Collares-Pereira for his idea of using a Sun multiplicator instead of doing the time-consuming work of identifying every optical error of our system.

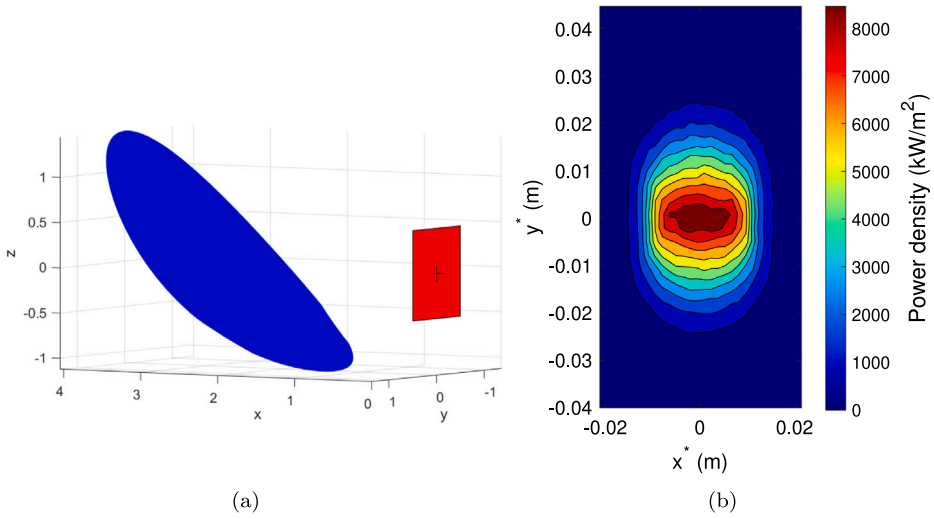

Fig. B.17. "Perfect" Scheffler reflector's shape (and inclined plane receiver) for a Sun at Zenith, A_{sc} = 8 m^2 and f_n = 1.43 m (a); Focal image that is obtained at equinox (b). P_{tot} = 4.74 kW ($\rho_{mirrors}$ = 0.9 and DNI = 900 W.m^{-2}).

Appendix A. Additional comments on the model

A.1. Differences with previous formulations

The present model follows the theoretical aspects that have been formulated by Reddy et al. [15], except that in the present work, the focal point of the parabola is fixed at the coordinate (x=0, y=0, z=0). This choice facilitates the mathematical developments, especially for rotations. It should be noted that the vertex of the imaginary paraboloid that is accommodated by the standing Scheffler reflector is usually located below the ground (*c.f.* Fig. 2), *i.e.* neither the height position of the receiver nor its distance to the reflector is equal to the focal distance of the parabola (although the distance between the focal point and the center of the reflector is supposed to be two times the focal distance [15]). Thus, without tangible meaning, the origin of the coordinate system does not matter.

A.2. Sun's position

The position of the Sun is calculated from the chosen latitude (lat), day and solar time, using simplified equations that can be found in [2]. A more complex "true" Sun position model could be used, such as the Solar Position Algorithm (SPA) from the NREL [36], but such accuracy is unnecessary for general calculations.

Appendix B. Continuous parabola

B.1. Ideal focal image

Another code has been developed and creates a continuous Scheffler reflector following the shape of a parabola, with no optical error and aiming at the Sun that is at the Zenith. Thus, the reference results that are pictured in Fig. B.17 show the best image that could be provided with an 8 m^2 Scheffler reflector, with a DNI of 900 W.m^{-2} and with a mirror reflectivity of 0.9. It should be noted that some limitation in the software prevent the user from having a non-zero declination, forbidding the use of this model for the parametric studies that motivated this work.

Results show in B.17-b that The image area is 26.4 cm^2 (100 % of P_{tot}) or 14.4 cm^2 (95% of P_{tot}) and the average power density 1975 kW.m^{-2} (100% of P_{tot}) or 3301 kW m^{-2} (95% of P_{tot}); CR are 2217 and 4076, respectively. These results are in good agreement with those from Reddy et al. [15], who developed an analytical model predicting the theoretical ideal shape of the image for different days and found a concentration ratio varying between 1000 (summer solstice) and 7000 (winter solstice) and with a value of ~4000 for the equinoxes, for a parabola of 8 m^2 with a focal length of 1.5 m.

The continuous reflector model shows the physical limits of the system. Although not representing the reality, it is a good reference for comparison with other simulations and experiments in order to seek for possible enhancement of the real systems. Thus, when compared to the model with facets, it shows that using flat mirrors strongly limits the possible concentration performance of the Scheffler reflector. Using aluminum thin sheets is a better option to accommodate the shape of the parabola.

B.2. Estimate of optical errors

Optical errors are the reason why actual reflectors do not reach theoretical focal images. It is therefore important to characterize these errors experimentally. In general, studies on concentrating technologies focus on the slope error, which is generally the most important one and give values < 4 mrad, for parabolic troughs [26,37], linear Fresnel [26, 38], parabolic dish [39,40], and central receiver technologies [26,41], the latter generally showing even lower values. Regarding Scheffler reflectors, thorough optical characterizations are lacking, but some values up to 12.0 mrad or even 26 mrad [19] have been reported [42].

The continuous parabola model has been used to study the influence of the optical errors on the focal image size, and results were compared to experimental ones in order to estimate the magnitude of the errors. Fig. B.18 shows the average power density received on a vertical 1 m^2 target, as well as the centroid position, with respect to k_{sun}. From these results, it is possible to roughly assess the total amount of experimental optical losses: the continuous parabola with $k_{sun,continuous}$ = 4.5 gives the same average power density $\langle\phi\rangle$ than the parabola with facets at equinox and with k_{sun} = 1. Using 0.1 m × 0.1 m mirror facets could therefore correspond to a total optical error of $\sigma_{tot,facet} = \sqrt{k_{sun,continuous}}\cdot\sigma_{sun} \approx 10$ mrad. Because another k_{sun} value of 7.2 has been found to match experimental and numerical results from the facet parabola, the total error is stronger. However, since interactions between the different errors are unknown, we can only roughly estimate the total value to 15 mrad - 25 mrad, confirming previous studies [19,42].

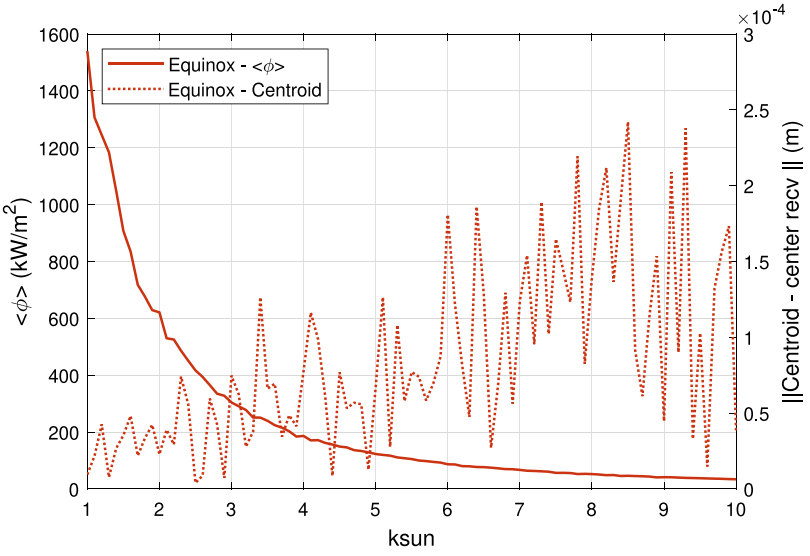

Fig. B.18. Ideal Scheffler parabola: Influence of k_{sun} on the size of the focal image for the equinoxes.

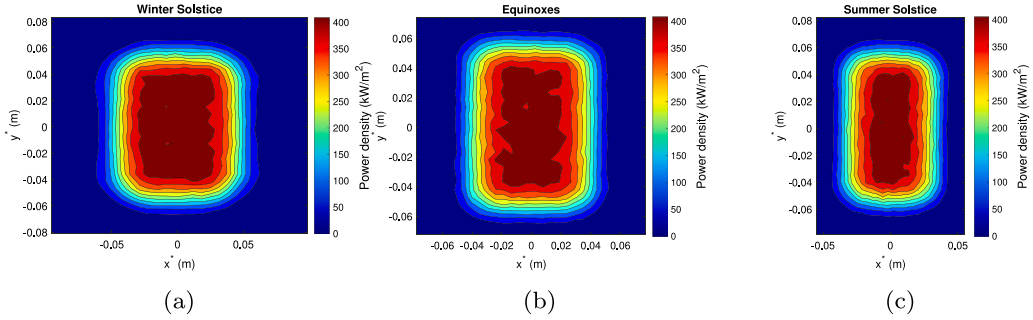

Fig. C.19. Variation of the numerical focal image with the declination with $k_{sun} = 1$: Winter solstice (a); Spring equinox (b); Summer solstice (c).

Appendix C. Results with other k_{sun}

One can build or experience a better Scheffler reflector, that is to say one giving smaller focal images. In order to assess the influence of the different parameters that were investigated in this study for different cases, the following subsections give the parametric study results for different values of k_{sun}, *i.e.* 1, 3, 5 and 9.

C.1. Results with $k_{sun} = 1$

The seasonal variations of the power densities with $k_{sun} = 1$ is given in Fig. C.19. Surprisingly, the focal image appears to be larger in winter than in summer, which is the opposite of the result obtained by [15,22]. One explanation could be that large, realistic reflectors ($A = 8$ m^2, $f = 1.43$ m) have such large optical errors that their whole behavior differs from that of small ($A = 2.7$ m^2, $f = 1$ m) and theoretical reflectors.

With $k_{sun} = 1$, the average power density received by the target $\langle\phi\rangle$ and the focal image's centroid position *vs.* the different adjustment errors are pictured in C.20. This represents a Scheffler parabola with 0.1 m × 0.1 m facets and no slope, specularity or shape errors. An almost perfect system like this one is very sensitive to the adjustment errors such as the South offset, the declination adjustment, the tracking, etc.

C.2. Results with $k_{sun} = 3$

With $k_{sun} = 3$, the average incident power density received by the target $\langle\phi\rangle$ and the focal image's centroid position *vs.* the different adjustment errors are pictured in C.21. This corresponds to a Scheffler parabola with 0.1 m × 0.1 m facets and small slope and specularity errors.

C.3. Results with $k_{sun} = 5$

With $k_{sun} = 5$, the average power density received by the target $\langle\phi\rangle$ and the focal image's centroid position *vs.* the different adjustment errors are pictured in C.22. This corresponds to a possible Scheffler parabola with 0.1 m × 0.1 m facets and better slope and specularity errors that the one we experimentally observed.

C.4. Results with $k_{sun} = 9$

With $k_{sun} = 9$, the average power density received by the target $\langle\phi\rangle$ and the focal image's centroid position *vs.* the different adjustment errors are pictured in C.23. This corresponds to a possible Scheffler parabola with 0.1 m × 0.1 m facets and worse slope and specularity errors that the one we experimentally observed. In this case, the system is really resilient to other errors.

Appendix D. Supplementary materials

The Soltrace script code has been deposited at OSF Home and is publicly available as of the date of publication. DOI is http://dx.doi.org/10.17605/OSF.IO/M3K7E.

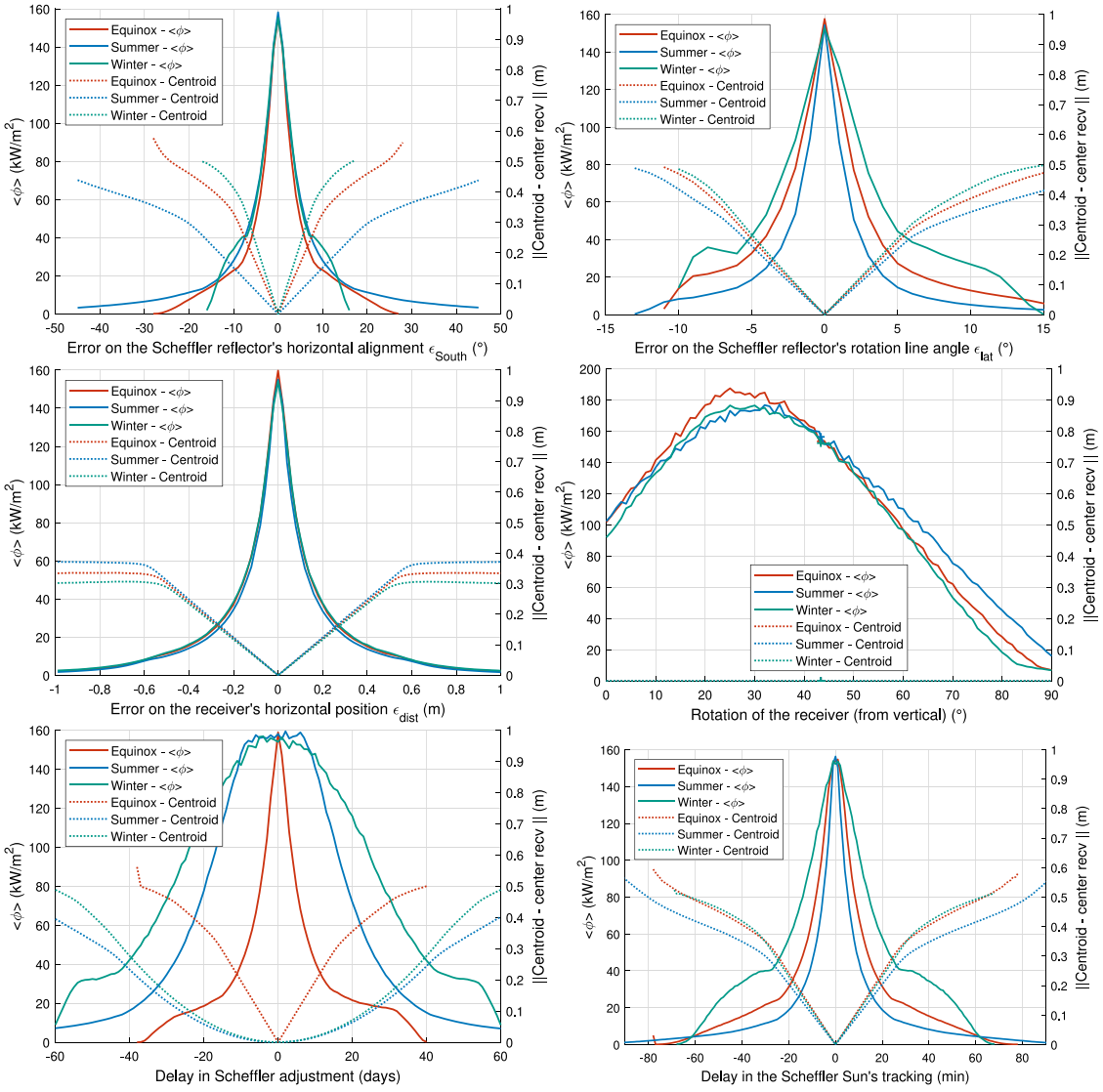

Fig. C.20. Average power density and centroid position with $k_{sun} = 1$.

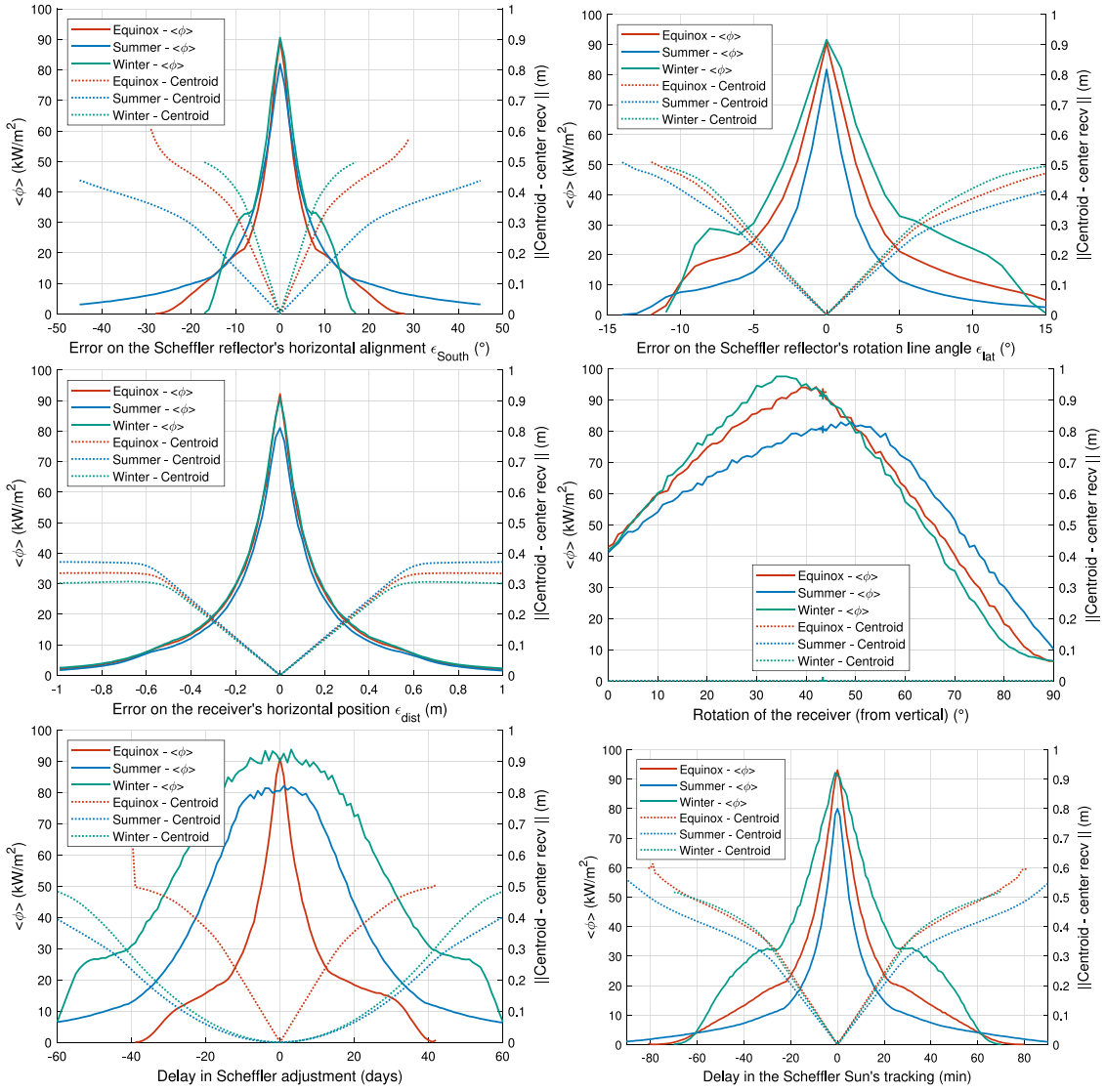

Fig. C.21. Average power density and centroid position with $k_{sun} = 3$.

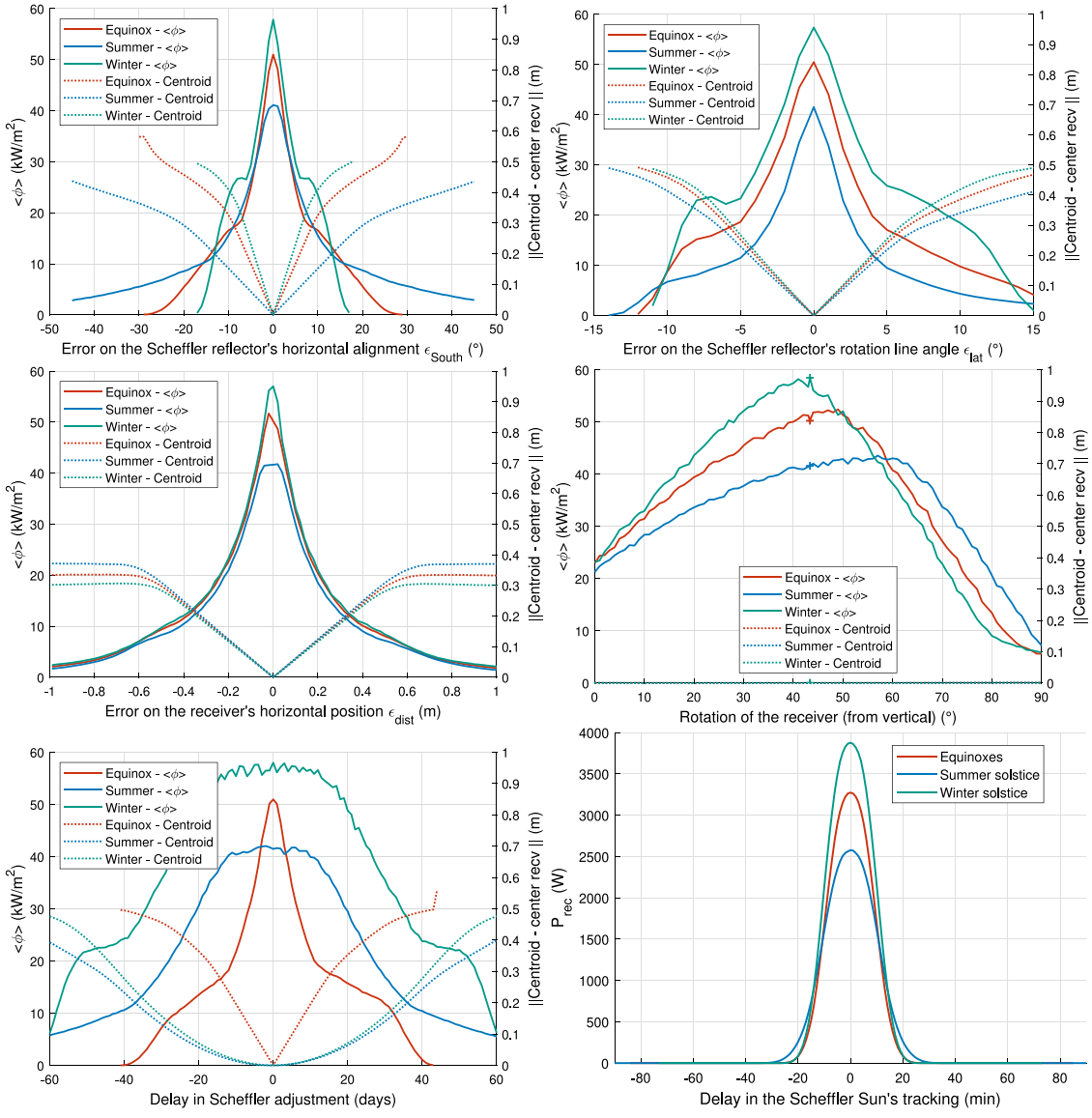

Fig. C.22. Average power density and centroid position with $k_{sun} = 5$.

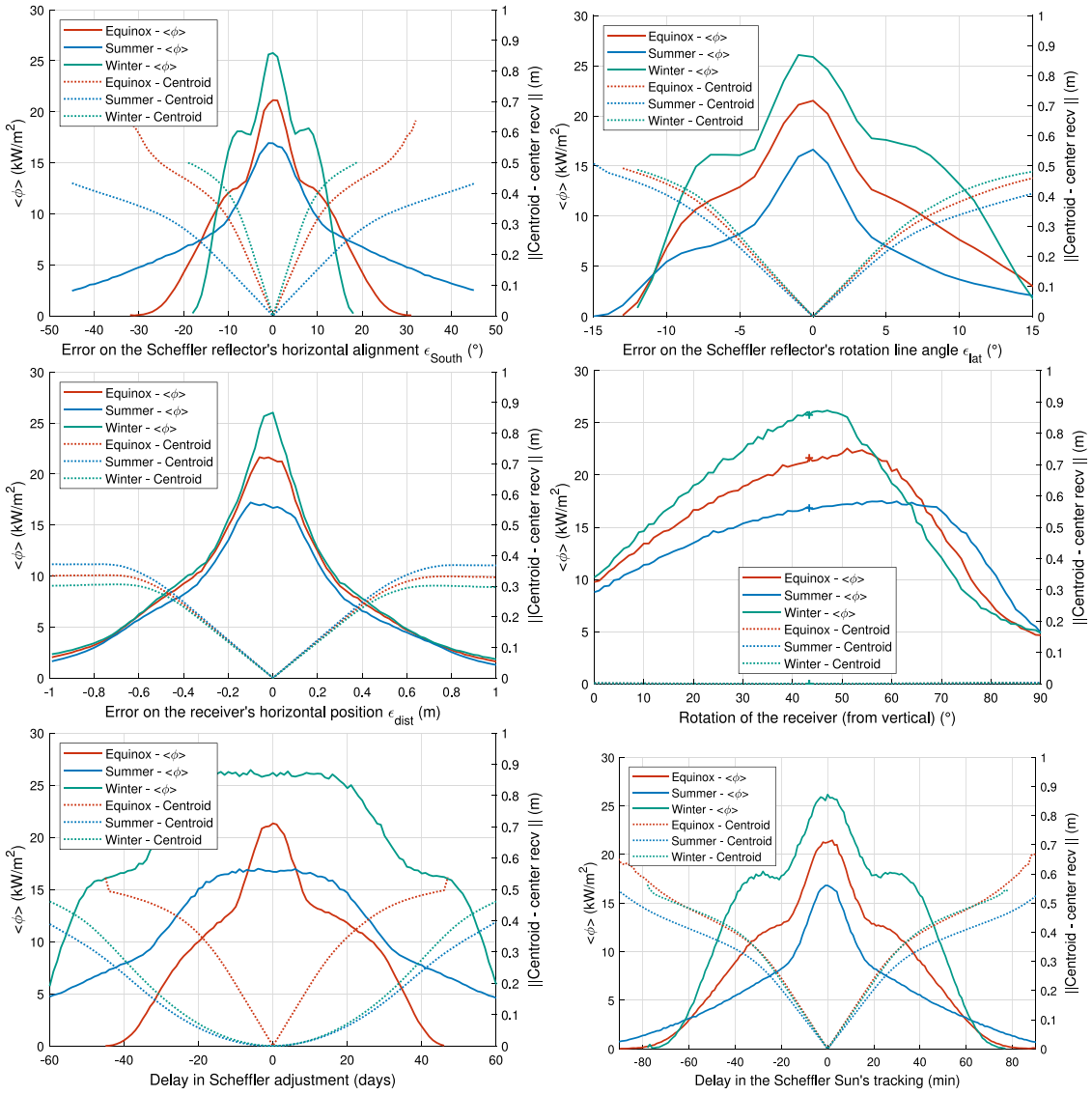

Fig. C.23. Average power density and centroid position with $k_{sun} = 9$.

References

[1] E. Guillot, R. Rodriguez, N. Boullet, J.-L. Sans, Some details about the third rejuvenation of the 1000 kWth solar furnace in Odeillo: Extreme performance heliostats, AIP Conf. Proc. 2033 (1) (2018) 040016, http://dx.doi.org/10.1063/1.5067052.

[2] S.A. Kalogirou, Solar Energy Engineering: Processes and Systems, second ed., Academic Press Elsevier, Kidlington, UK, 2014.

[3] W. Scheffler, Introduction to the revolutionary design of Scheffler reflectors, in: Proceedings of the Solar Cookers and Food Processing International Conference, Granada, Spain, 2006, p. 4.

[4] U. Oelher, W. Scheffler, The use of indigenous materials for solar conversion, Sol. Energy Mater. Sol. Cells 33 (3) (1994) 379–387, http://dx.doi.org/10.1016/0927-0248(94)90239-9.

[5] W. Scheffler, Development of a solar crematorium, in: Proceedings of the Solar Cookers and Food Processing International Conference, Granada, Spain, 2006, p. 2.

[6] H. Panchal, J. Patel, K. Parmar, M. Patel, Different applications of Scheffler reflector for renewable energy: A comprehensive review, Int. J. Ambient. Energy 41 (6) (2018) 716–728, http://dx.doi.org/10.1080/01430750.2018.1472655.

[7] A. Kumar, O. Prakash, A.K. Kaviti, A comprehensive review of Scheffler solar collector, Renew. Sustain. Energy Rev. 77 (2017) 890–898, http://dx.doi.org/10.1016/j.rser.2017.03.044.

[8] F.J. Barba, M. Gavahian, I. Es, Z. Zhu, F. Chemat, J.M. Lorenzo, A. Mousavi Khaneghah, Solar radiation as a prospective energy source for green and economic processes in the food industry: From waste biomass valorization to dehydration, cooking, and baking, J. Clean. Prod. 220 (2019) 1121–1130, http://dx.doi.org/10.1016/j.jclepro.2019.02.175.

[9] A. Chandak, S.K. Somani, D. Dubey, Design, development and testing of multieffect distiller/evaporator using Scheffler solar concentrators, J. Eng. Sci. Technol. 4 (3) (2009) 315–321.

[10] Q. Alkhalaf, A.R.S. Suri, S.S. Chandel, S. Thapa, M.S.A. Ansari, Performance investigation of a Scheffler solar cooking system combined with stirling engine, Mater. Today: Proc. (2023) http://dx.doi.org/10.1016/j.matpr.2023.01.399.

[11] H. Naik, P. Baredar, A. Kumar, Medium temperature application of concentrated solar thermal technology: Indian perspective, Renew. Sustain. Energy Rev. 76 (2017) 369–378, http://dx.doi.org/10.1016/j.rser.2017.03.014.

[12] S. Indora, T.C. Kandpal, Institutional cooking with solar energy: A review, Renew. Sustain. Energy Rev. 84 (2018) 131–154, http://dx.doi.org/10.1016/j.rser.2017.12.001.

[13] T. Kanyowa, G.V. Nyakujara, E. Ndala, S. Das, Performance analysis of Scheffler dish type solar thermal cooking system cooking 6000 meals per day, Sol. Energy 218 (2021) 563–570, http://dx.doi.org/10.1016/j.solener.2021.03.019.

[14] A. Munir, O. Hensel, W. Scheffler, Design principle and calculations of a Scheffler fixed focus concentrator for medium temperature applications, Sol. Energy 84 (8) (2010) 1490–1502, http://dx.doi.org/10.1016/j.solener.2010.05.011.

[15] D.S. Reddy, M.K. Khan, M.Z. Alam, H. Rashid, Design charts for Scheffler reflector, Sol. Energy 163 (2018) 104–112, http://dx.doi.org/10.1016/j.solener.2018.01.081.

[16] D.S. Reddy, M.K. Khan, Design and ray tracing of multifaceted Scheffler reflector with novel crossbars, Sol. Energy 185 (2019) 363–373, http://dx.doi.org/10.1016/j.solener.2019.04.083.

[17] J. Ruelas, G. Pando, B. Lucero, J. Tzab, Ray tracing study to determine the characteristics of the solar image in the receiver for a Scheffler-type solar concentrator coupled with a stirling engine, in: Proceedings of the ISES Solar World Congress 2013, in: Energy Procedia, vol. 57, Elsevier, Cancún, Mexico, 2014, pp. 2858–2866, http://dx.doi.org/10.1016/j.egypro.2014.10.319.

[18] J. Ruelas, J. Palomares, G. Pando, Absorber design for a Scheffler-type solar concentrator, Appl. Energy 154 (2015) 35–39, http://dx.doi.org/10.1016/j.apenergy.2015.04.107.

[19] S. Sasidharan, P. Dutta, Optical characterization of a fixed focus Scheffler reflector for pressurized solar receiver testing, Sol. Energy 227 (2021) 89–100, http://dx.doi.org/10.1016/j.solener.2021.08.078.

[20] D. Fontani, P. Sansoni, F. Francini, F. Toni, D. Jafrancesco, Optical raytracing analysis of a Scheffler type concentrator, Energies 15 (1) (2022) 260, http://dx.doi.org/10.3390/en15010260.

[21] G. Guillet, J. Gaspar, S. Barbosa, T. Fasquelle, B. Kadoch, Experimental evaluation of the concentrated solar heat flux distribution provided by an 8 m2 Scheffler reflector, Renew. Energy 223 (2024) 119958, http://dx.doi.org/10.1016/j.renene.2024.119958.

[22] E.A. Dib, Análise Da Formação De Imagem Focal Do Concentrador Solar Paraboloidal Tipo Scheffler (Ph.D. thesis), Universidade de São Paulo, São Paulo, Brazil, 2021, http://dx.doi.org/10.11606/T.3.2021.tde-24112021-140456.

[23] T. Wendelin, SolTRACE: A new optical modeling tool for concentrating solar optics, in: Proceedings of the International Solar Energy Conference 2003, American Society of Mechanical Engineers Digital Collection, Kohala Coast, HI, USA, 2003, pp. 253–260, http://dx.doi.org/10.1115/ISEC2003-44090.

[24] D. Jafrancesco, J.P. Cardoso, A. Mutuberria, E. Leonardi, I. Les, P. Sansoni, F. Francini, D. Fontani, Optical simulation of a central receiver system: Comparison of different software tools, Renew. Sustain. Energy Rev. 94 (2018) 792–803, http://dx.doi.org/10.1016/j.rser.2018.06.028.

[25] A. Malan, K. Ravi Kumar, A comprehensive review on optical analysis of parabolic trough solar collector, Sustain. Energy Technol. Assess. 46 (2021) 101305, http://dx.doi.org/10.1016/j.seta.2021.101305.

[26] N. Kincaid, G. Mungas, N. Kramer, M. Wagner, G. Zhu, An optical performance comparison of three concentrating solar power collector designs in linear Fresnel, parabolic trough, and central receiver, Appl. Energy 231 (2018) 1109–1121, http://dx.doi.org/10.1016/j.apenergy.2018.09.153.

[27] A. Carrillo-Andrés, X. Apaolaza-Pagoaga, C.R. Ruivo, E. Rodríguez-García, F. Fernández-Hernández, Optical characterization of a funnel solar cooker with Azimuthal sun tracking through ray-tracing simulation, Sol. Energy 233 (2022) 84–95, http://dx.doi.org/10.1016/j.solener.2021.12.027.

[28] M.J. Wagner, T. Wendelin, Solarpilot: A power tower solar field layout and characterization tool, Sol. Energy 171 (2018) 185–196, http://dx.doi.org/10.1016/j.solener.2018.06.063.

[29] K. Lovegrove, W. Stein, Concentrating solar power technology: Principles, developments and applications, in: Energy, no. 21, first ed., Woodhead Publishing, Cambridge, UK, 2012.

[30] K. Pottler, E. Lüpfert, G.H.G. Johnston, M.R. Shortis, Photogrammetry: A powerful tool for geometric analysis of solar concentrators and their components, J. Sol. Energy Eng. 127 (1) (2005) 94–101, http://dx.doi.org/10.1115/1.1824109.

[31] M. El Ydrissi, H. Ghennioui, E.G. Bennouna, A. Farid, A review of optical errors and available applications of deflectometry technique in solar thermal power applications, Renew. Sustain. Energy Rev. 116 (2019) 109438, http://dx.doi.org/10.1016/j.rser.2019.109438.

[32] B. Iooss, P. Lemaître, A review on global sensitivity analysis methods, in: G. Dellino, C. Meloni (Eds.), Uncertainty Management in Simulation-Optimization of Complex Systems: Algorithms and Applications, in: Operations Research/Computer Science Interfaces Series, (no. 59) Springer, Boston, MA, USA, 2015, pp. 101–122, http://dx.doi.org/10.1007/978-1-4899-7547-8_5, chapter number: 5.

[33] S. Launay, B. Kadoch, O. Le Métayer, C. Parrado, Analysis strategy for multi-criteria optimization: Application to inter-seasonal solar heat storage for residential building needs, Energy 171 (2019) 419–434, http://dx.doi.org/10.1016/j.energy.2018.12.181.

[34] D.C. Montgomery, Design and analysis of experiments, eighth ed., Wiley, Hoboken, NJ, USA, 2013.

[35] J. Chaves, Introduction to Nonimaging Optics, CRC Press, 2008.

[36] I. Reda, A. Andreas, Solar position algorithm for solar radiation applications, Sol. Energy 76 (5) (2004) 577–589, http://dx.doi.org/10.1016/j.solener.2003.12.003.

[37] T. Wendelin, Parabolic Trough VSHOT Optical Characterization in 2005–2006, Incline Village, NV, USA, 2006.

[38] M. Hack, G. Zhu, T. Wendelin, Evaluation and comparison of an adaptive method technique for improved performance of linear Fresnel secondary designs, Appl. Energy 208 (2017) 1441–1451, http://dx.doi.org/10.1016/j.apenergy.2017.09.009.

[39] C.E. Andraka, Cost/performance tradeoffs for reflectors used in solar concentrating dish systems, in: Proceedings of the 2nd International Conference on Energy Sustainability, American Society of Mechanical Engineers Digital Collection, Jacksonville, FL, USA, 2008, pp. 505–513, http://dx.doi.org/10.1115/ES2008-54048.

[40] M. Shortis, G. Johnston, Photogrammetry: An available surface characterization tool for solar concentrators, part II: Assessment of surfaces, J. Sol. Energy Eng. 119 (4) (1997) 286–291, http://dx.doi.org/10.1115/1.2888034.

[41] F. Arqueros, A. Jiménez, A. Valverde, A novel procedure for the optical characterization of solar concentrators, Sol. Energy 75 (2) (2003) 135–142, http://dx.doi.org/10.1016/j.solener.2003.07.008.

[42] J. Ruelas, N. Velázquez, J. Cerezo, A mathematical model to develop a Scheffler-type solar concentrator coupled with a stirling engine, Appl. Energy 101 (2013) 253–260, http://dx.doi.org/10.1016/j.apenergy.2012.05.040.